THE UNIVERSITY OF
WARWICK

University of Warwick institutional repository: http://go.warwick.ac.uk/wrap

This paper is made available online in accordance with
publisher policies. Please scroll down to view the document
itself. Please refer to the repository record for this item and our
policy information available from the repository home page for
further information.

To see the final version of this paper please visit the publisher's website.
Access to the published version may require a subscription.

Author(s): M. E. Dieckmann, G. Rowlands, B. Eliasson, and P. K. Shukla

Article Title: Particle-in-cell simulations of electron acceleration by a simple capacitative antenna in collisionless plasma
Year of publication: 2004
Link to published article:
http://dx.doi.org/10.1029/2004JA010436
Publisher statement: An edited version of this paper was published by AGU. Copyright (2004) American Geophysical Union.
M. E. Dieckmann, G. Rowlands, B. Eliasson, and P. K. Shukla (2004), Particle-in-cell simulations of electron acceleration by a simple capacitative antenna in collisionless plasma, Journal of Geophysical Research, Vol. 109, A12304, doi:10.1029/2004JA010436. To view the published open abstract, go to http://dx.doi.org and enter the DOI.

Particle-in-cell simulations of electron acceleration by a simple capacitative antenna in collisionless plasma

M. E. Dieckmann[1]
Institut für Theoretische Physik IV, Ruhr-Universität Bochum, Bochum, Germany

G. Rowlands
Department of Physics, University of Warwick, Coventry, UK

B. Eliasson and P. K. Shukla
Institut für Theoretische Physik IV, Ruhr-Universität Bochum, Bochum, Germany

Received 13 February 2004; revised 3 September 2004; accepted 12 October 2004; published 10 December 2004.

[1] We examine the electron acceleration by a localized electrostatic potential oscillating at high frequencies by means of particle-in-cell (PIC) simulations, in which we apply oscillating electric fields to two neighboring simulation cells. We derive an analytic model for the direct electron heating by the externally driven antenna electric field, and we confirm that it approximates well the electron heating obtained in the simulations. In the simulations, transient waves accelerate electrons in a sheath surrounding the antenna. This increases the Larmor radii of the electrons close to the antenna, and more electrons can reach the antenna location to interact with the externally driven fields. The resulting hot electron sheath is dense enough to support strong waves that produce high-energy sounder-accelerated electrons (SAEs) by their nonlinear interaction with the ambient electrons. By increasing the emission amplitudes in our simulations to values that are representative for the ones of the sounder on board the OEDIPUS C (OC) satellites, we obtain electron acceleration into the energy range which is comparable to the 20 keV energies of the SAE observed by the OC mission. The emission also triggers stable electrostatic waves oscillating at frequencies close to the first harmonic of the electron cyclotron frequency. We find this to be an encouraging first step of examining SAE generation with kinetic numerical simulation codes. *INDEX TERMS:* 2451 Ionosphere: Particle acceleration; 2483 Ionosphere: Wave/particle interactions; 7819 Space Plasma Physics: Experimental and mathematical techniques; *KEYWORDS:* antenna, sounder-accelerated electrons, particle-in-cell simulation

Citation: Dieckmann, M. E., G. Rowlands, B. Eliasson, and P. K. Shukla (2004), Particle-in-cell simulations of electron acceleration by a simple capacitative antenna in collisionless plasma, *J. Geophys. Res.*, *109*, A12304, doi:10.1029/2004JA010436.

1. Introduction

[2] Increased numbers of heated electrons have repeatedly been observed in the energy band of 20 eV to 20 keV by the two-satellite mission OEDIPUS C (OC), after the emission of a strong wave pulse into the ambient plasma of the topside ionosphere. A clear correlation has been found between the spacecraft separation and the time interval between the emission by the sounding satellite and the observation of energetic electrons by the receiving satellite [*James et al.*, 1999; *Huang et al.*, 2001], indicating that these electrons are sounder-accelerated electrons (SAEs).

[3] The strongest electron heating has been observed when the emission frequency is in the same frequency interval as some eigenmode of the plasma, such as electron whistlers or electron Bernstein modes, suggesting that these eigenmodes are involved in the electron heating mechanism. The electrons could be heated by nonlinear wave-particle interactions [*Pulinets and Selegey*, 1986; *Shuiskaya et al.*, 1990]; however, *James et al.* [1999] argued that this process may not work for the OC sounder. They arrived at this conclusion by considering strong Langmuir turbulence described within the framework of the Zakharov equations, which ignored a possible increase of the electron thermal energy density due to the interaction of the electrons with the vacuum potential, the very near field (VNF), of the antenna or linearly damped transient wave modes which we here call the near field. The electron heating would increase the effective plasma temperature, allowing for larger wave electric fields close to the antenna, and plasma wave turbulence could then accelerate electrons to significantly higher energies than the ones estimated by *James et al.* [1999].

[4] A theoretical examination of the electron acceleration by the OC antenna fields is problematic, in particular with

[1]Also at Department of Science and Technology, Linköpings University, Campus Norrköping, Sweden.

Copyright 2004 by the American Geophysical Union.
0148-0227/04/2004JA010436$09.00

respect to strong plasma wave turbulence, since the shape and the magnitude of the near field potential and its coupling to the propagating wave modes of the antenna far field has not yet unambiguously been derived [*James et al.*, 1999]. For emission frequencies close to the harmonics of the electron gyrofrequency, the far field properties may also be modified by the nonlinear Landau damping of electron Bernstein waves propagating transverse to the magnetic field direction [*Riyopoulos*, 1986] or by the linear Landau damping for obliquely propagating waves. It is also difficult to measure the electric field distribution around the antenna, and the antenna impedance can often only be estimated from the absorption of energy by the surrounding plasma [*James et al.*, 1999; *Tsutsui et al.*, 1997; *Kellogg and Bale*, 2001].

[5] Particle-in-cell (PIC) simulations can, in principle, provide a powerful tool to examine the electron acceleration by the OC antenna, but the modeling of a fully three-dimensional (3-D) antenna at the required spatiotemporal resolution with a sufficient number of particles per cell is computationally extremely demanding. It is, however, possible to examine the electron acceleration by a simplified antenna model, and with the ever-increasing computer speed we can then progressively refine our antenna model to make it more realistic. This work constitutes an initial step toward this goal.

[6] We model the antenna as an oscillating charge density and we exclude magnetic fields generated by the antenna currents. Our antenna is thus purely electrostatic (ES). We have previously examined the coupling between an antenna and a plasma using this model for the emission of waves with frequencies close to the upper-hybrid resonance frequency and to the maxima of the electron Bernstein mode. In previous works [*Dieckmann et al.*, 1999; *Dieckmann et al.*, 2000] we have found that electrons are heated by the antenna emission, but we have not unambiguously identified the underlying mechanism. In the present work we have found that the antenna VNF and the damping of the transient wave modes driven by the antenna play an important role in the heating. The transient waves form a high-frequency sheath around the antenna in which electrons are accelerated. The electron heating by the transient wave modes expands their Larmor radius and they can reach the antenna from a larger distance. By this heating mechanism, the antenna and its VNF can couple energy to a larger spatial volume.

[7] The paper is organized in the following manner. In section 2 we derive an analytic map for the interaction between the electrons and a piecewise constant electric field, which represents the unshielded VNF of the simple antenna in our simulation. This map gives us the maximum speed that the electrons can reach by interacting with our simulation antenna. In section 3 we perform numerical simulations where we apply electric field amplitudes to our simulation antenna for which our analytic estimate fits best and which are in the same regime as the emission amplitudes that have been used in previous works [*Dieckmann et al.*, 1999; *Dieckmann et al.*, 2000]. We examine the coupling of the antenna to the plasma for an emission frequency that is twice the electron cyclotron frequency due to its important role as a resonance frequency for plasma sounders. We find that the electrons are heated close to the antenna by the near field and by the VNF. We further find slowly propagating or nonpropagating ES oscillations at the emission frequency. These oscillations may be connected to the strong plasma response to sounding at the harmonics of the electron cyclotron frequency. In section 4 we increase the emission amplitude to values that might be comparable to those the OC sounder uses. We observe the formation of a sheath of hot electrons where some electrons can reach peak energies of 1 keV, providing evidence that SAE can be generated by the VNF of the OC antenna, as proposed by *James et al.* [1999], and by the damping of transient waves driven by the antenna. The beams of heated electrons may drive and support the observed large-amplitude sheath waves [*James*, 1993; *James et al.*, 1995]. Wave-particle interactions with these strong sheath waves may then further accelerate the electrons to the observed energies of 20 keV. We summarize and discuss the results in section 5.

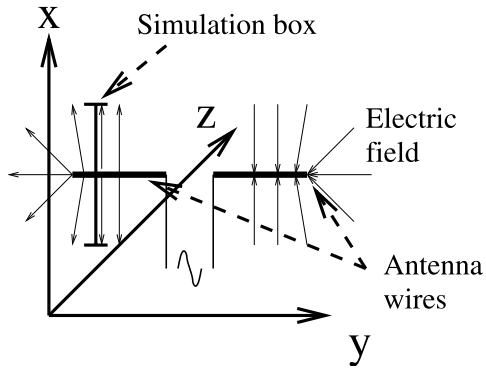

Figure 1. Our dipole antenna model. We apply an external time-oscillating current to both antenna wires, which in our one-dimensional (1-D) simulation geometry are represented by plates extended in the *y*-*z* plane. Our 1-D simulation box is orthogonal to the antenna wires (plates) and is placed close to the tip of the left antenna, as indicated by the vertical line parallel to the $x-$axis. Here, the current-induced magnetic force acting on the electrons is assumed to be negligibly small compared with the electric force of the radial electric field. We assume that the electric field varies only along the $x-$axis, and variations along *y* and *z* and are thus not represented in the model. The time-independent background magnetic field is aligned with the $z-$axis. The vectors indicate the direction of the electric field generated by the antenna at a particular time in the *x*-*y* plane.

2. Electron Acceleration by the Antenna Vacuum Potential

[8] We consider a purely ES interaction between an antenna with an externally driven, time-oscillating electric potential and the ambient electrons in one spatial dimension. The mean potential of our antenna is zero relative to that of the surrounding plasma. Since we consider a 1-D geometry on a Cartesian grid, our antenna corresponds to a thin plate extended perpendicular to the *x* direction. We do not introduce oscillating external currents and we thus exclude time-oscillating antenna magnetic fields. We do however consider a uniform background magnetic field. We set this field to $\mathbf{B} = B_0\mathbf{x_z}$, where $\mathbf{x_z}$ is the unit vector in the *z* direction. Our chosen simplified antenna model is shown in Figure 1.

[9] The Debye radius in plasmas is $\lambda_D = \{\epsilon_0 k_B T/ne^2\}^{1/2}$, where ϵ_0, k_B, T, n, and e are the electric permittivity, the Boltzmann constant, the electron temperature, the electron number density, and the amplitude of the electron charge, respectively. We assume that the electrons initially have an isothermal Maxwellian velocity distribution with the thermal speed $v_{th} = (k_B T/m)^{1/2}$, where m is the electron mass. The electron plasma and electron gyrofrequencies are $\omega_p = \lambda_D^{-1} v_{th}$ and $\omega_c = -e|\mathbf{B}|/m$, respectively.

[10] We normalize the variables into dimensionless, primed units; accordingly, the time is normalized as $t = \omega_p^{-1} t'$, the spatial coordinate is normalized as $x = \lambda_D x'$, the velocity is normalized as $v = v_{th} v'$, and the electric field is normalized as $E = v_{th}(n_0 m/\epsilon_0)^{1/2} E'$. We refer to the normalized velocity component along the simulation direction as v'_x and to the speed modulus perpendicular to the magnetic field as $v'_\perp = v_{th}^{-1}\sqrt{v_x^2 + v_y^2}$. The electron gyrofrequency is normalized as $\omega_c = \omega_p \omega'_c$, and the emission frequency of the antenna (to be discussed below) is normalized as $\omega_e = \omega_p \omega'_e$. In the following, we will use the dimensionless units, if not stated otherwise, and we will drop the primes.

[11] The nonrelativistic equation of motion for an electron moving along the x direction in the presence of the electric field $E(x, t)$ and a constant background magnetic field is of the form

$$\frac{d^2 v_x}{dt^2} = -\frac{dE}{dt} - \omega_c^2 v_x, \tag{1}$$

where $x(t)$ and $v_x(t)$ are the x coordinate and velocity, respectively. We assume that the VNF very close to the antenna is unshielded by the plasma and we approximate it by a piecewise constant electric field $E(x, t) = E_0 \sin(\omega_e t)[2H(x) - H(x-1) - H(x+1)]$ in x direction, where ω_e is the emission frequency of the antenna and the Heaviside function takes the value $H(x) = 1$ for $x > 0$ and $H(x) = 0$ for $x < 0$. We have used the same approximation for the antenna electric field in the PIC simulation. We also assume that the force exerted by the VNF on the electrons is large compared with the magnetic field contribution (neglecting the $\omega_c^2 v_x$ term in equation (1)), giving

$$\frac{d^2 x}{dt^2} = E_0 \sin(\omega_e t), \qquad -1 \le x < 0 \tag{2}$$

$$\frac{d^2 x}{dt^2} = -E_0 \sin(\omega_e t), \qquad 0 \le x \le 1. \tag{3}$$

[12] We now let an electron enter the VNF at the time $t = t_0$ at the position $x_0 = -1$ with the speed $v_{x,0}$. The solution of equation (2) gives the time-dependent position of the electron in the interval $-1 \le x \le 0$ as

$$x(t) = -1 + v_{x,0}(t - t_0) - \frac{E_0}{\omega_e}\left[\frac{\sin(\omega_e t)}{\omega_e} - \frac{\sin(\omega_e t_0)}{\omega_e} - \cos(\omega_e t_0)(t - t_0)\right]. \tag{4}$$

Assuming that the VNF region is small, we obtain $\omega_e(t - t_0) \ll 1$. Taylor-expanding the sine function to second order in $\omega_e(t - t_0)$, equation (4) yields

$$x \approx -1 + v_{x,0}(t - t_0) + \frac{E_0}{2}\sin(\omega_e t_0)(t - t_0)^2. \tag{5}$$

[13] The electron arrives at $x = 0$ at the time $\tilde{t} = t_0 + v_{x,0}^{-1}[1 - E_0 \sin(\omega_e t_0)/2v_{x,0}^2]$, or at the approximate time $t_1 = t_0 + v_{x,0}^{-1}$ if $E_0/2v_{x,0}^2 \ll 1$, which we denote "condition 1." Differentiating equation (5) with respect to time and using the approximate travel time $t_1 - t_0 = v_{x,0}^{-1}$, we obtain

$$v_{x,1} = v_{x,0}\left[1 + \frac{E_0 \sin(\omega_e t_0)}{v_{x,0}^2}\right], \tag{6}$$

which relates the exit velocity $v_{x,1}$ to the entrance velocity $v_{x,0}$. We can now find the particle motion in the region $0 \le x \le 1$ by simply substituting $E_0 \to -E_0$, $t_0 \to t_1$, and $v_{x,0} \to v_{x,1}$ into equation (4). Then we obtain the approximate arrival time of the electron at $x = 1$ as $t_2 = t_0 + v_{x,0}^{-1} + v_{x,1}^{-1}$, which can be substituted into equation (6) to obtain the speed $v_{x,2}$ in terms of $v_{x,1}$. By combining the maps $v_{x,0} \to v_{x,1}$ with $v_{x,1} \to v_{x,2}$, we obtain to lowest order the map $v_{x,0} \to v_{x,2}$, namely,

$$v_{x,2} = v_{x,0}\left[1 - \frac{\omega_e E_0 \sin(2\omega_e t_0)}{2v_{x,0}^3}\right], \tag{7}$$

and, subsequently, find the passage time $t_2 - t_0 \approx 2/v_{x,0}$. By comparing the magnitude of the lowest-order velocity changes due to the electric field given by equation (7) to the corresponding lowest-order velocity changes by the magnetic field given by $d^2x/dt^2 = -\omega_c v_x$, we find that equation (7) is valid as long as $|E_0/v_{x,0}\omega_c| \gg 1$, which we denote "condition 2." Note that this model is valid only as long as the gyroradius of the electrons is significantly larger than the antenna width.

[14] The term t_0 in equation (7) shows that the acceleration depends on the antenna phase when the electron enters the VNF. In the presence of many electrons with differing initial phases we may obtain a randomization of the electron trajectories, which likely leads to the heating of electrons. Since the electron mobility across the magnetic field is low, the antenna accelerates primarily electrons in our 1-D model that gyrate around a center located within a thermal gyroradius from the antenna.

3. Numerical Simulations

[15] In the numerical solutions, the Vlasov-Maxwell equations are solved self-consistently in one spatial dimension (along the x direction) and three velocity dimensions, by means of PIC simulations. We use a grid for the piecewise constant electric and magnetic fields and approximate the plasma by an ensemble of computational particles [*Eastwood*, 1991]. In what follows, we only consider the electric field component of the ES field in $x-$direction. Periodic boundary conditions are used in the x space, and we reduce finite-box effects by choosing a large enough normalized box length of $L = 800$. We consider the high emission frequency $\omega_e = 2|\omega_c|$ and a short emission duration $T_e = 80\pi$, allowing us to represent the positive ions by an immobile positive charge background. We choose the magnetic field so that $\omega_c = -0.25$. Unless stated otherwise, we use 409,600 computational electrons which are initially distributed uniformly in space and which have a Maxwellian velocity distribution. With the chosen number of electrons, velocity space is initially populated up to a

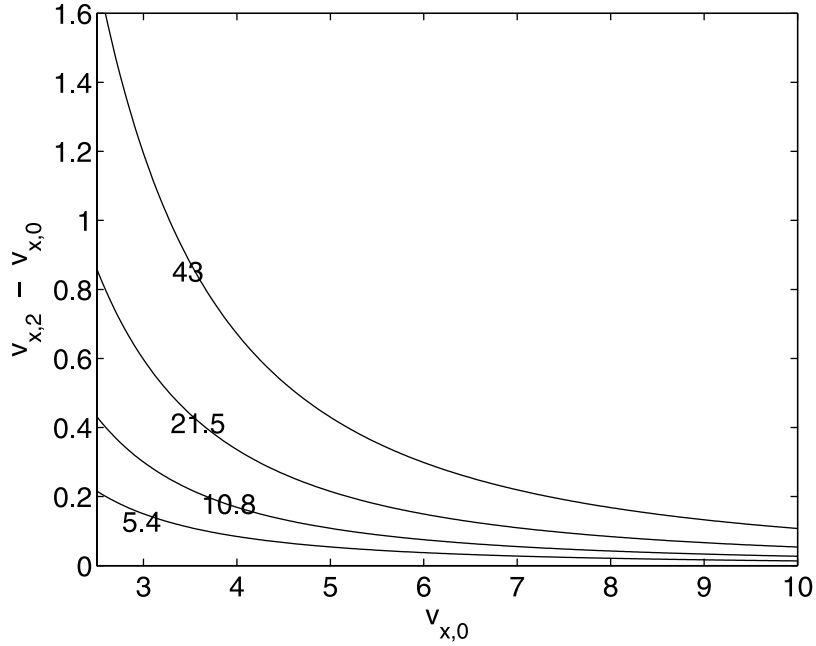

Figure 2. The maximum speed increment $v_{x,2} - v_{x,0}$ an electron can gain by crossing the antenna once, as a function of the initial speed $v_{x,0}$, for the emission amplitudes $E_{0,1} = 5.4$, $E_{0,2} = 10.8$, $E_{0,3} = 21.5$ and $E_{0,4} = 43$. If we initially set $v_y = 0$, then our assumption of a weak magnetic field allows us to take $v_\perp \approx v_x$ during the time the electron interacts with the antenna. Note that the accuracy of the map we use decreases for decreasing v_x and for increasing E_0. We have thus not shown its solution for $v_x < 2.5$.

maximum velocity $v_{\perp,\max} \approx 3.5$. The mass ratio between a computational electron with mass m_c and a physical electron with mass m of $m_c/m \approx 10^7$ leads to ES noise in the simulations with amplitudes that are $(m_c/m)^{0.5}$ times higher than the thermal noise in plasma provided that the scaling is comparable to that in unmagnetized plasma [*Dieckmann et al.*, 2004]. Our signal to noise ratio is thus limited.

[16] During the emission time $t < T_e$, we apply an oscillating electric field in x direction to the two simulation cells which represent the antenna, located in the spatial interval between $x = -1$ and $x = 1$. While this external field is immersed in plasma, we can neglect the relatively small plasma response to this field at these cells, and we therefore refer to the potential of the external fields as the vacuum potential since it is not affected by the plasma. We examine the electron acceleration for the emission frequency $\omega_e = 0.5$ and for four different electric field amplitudes $E_{0,1} = 5.4$, $E_{0,2} = 10.8$, $E_{0,3} = 21.5$, and $E_{0,4} = 43$. For the fastest electrons, moving with velocity $v_\perp$,max and $v_y = 0$, condition 1 reads $E_0 \ll 24$ which is approximately fulfilled by the fields $E_{0,1}$ and $E_{0,2}$. For the largest $v_{\perp,\max}$ the condition 2 reads $E_0 \gg 1.15$ which is approximately fulfilled for all fields. As we show below, the electrons are heated by the emission, and their increased speeds will make the map (7) applicable also to the fields $E_{0,3}$ and $E_{0,4}$.

[17] In Figure 2 we show the solution of equation (7) for the four emission amplitudes. We calculate how much the electron increases its v_x-speed if it encounters the antenna at the optimum phase and with $v_y = 0$. We notice that the acceleration curves rapidly drop for increasing initial v_x and even for the emission amplitude $E_{0,4}$ we do not expect any rapid electron acceleration beyond $v_x \approx 10$, even for multiple antenna crossings at the optimum phase.

[18] Our PIC simulations follow the evolution of the plasma up to the end time $T_t = 186\pi$. We compare the solution of the linear dispersion relation for the given plasma parameters to the ES fields in the simulations that are developed in response to the $E_{0,1}$ emission. In Figure 3 we have Fourier transformed the simulation ES field over space and time for two time intervals with a respective duration of T_e. In the time interval between $t = 0$ and $t = T_e$, we identify an intense broadband structure at frequencies close to $\omega = 2\omega_c$ as the emission pulse. The short duration and the spatial localization of the emission distributes the emitted wave power over a large ω, k interval. The components of the emission spectrum which are not linearly undamped Bernstein mode waves are absorbed. This absorption depends on ω and k. Interesting is that Figure 3a shows also a second band of the emission close to the Bernstein mode branch between $\omega = \omega_c$ and $\omega = 2\omega_c$. The frequency spread of the emission has been sufficient to excite waves in this lower Bernstein mode band while the transient waves at $\omega \approx 1.5\omega_c$ appear to be strongly damped. The emission pulse has been absorbed by the electrons until the simulation's end. As we can see in Figure 3b, the broadband wave pulse has vanished. Figure 3 further shows waves with values for ω and k that match those of the linearly undamped Bernstein mode waves.

[19] We now examine the spatial distribution of the emitted waves in the simulation. We obtain this distribution by a Fourier transformation over time of the ES field and the extraction of the amplitude moduli for the frequency ω_e. In Figure 4 we show the logarithmic amplitude modulus of the waves driven by the four antenna fields $E_{0,j}$ and for the time interval between $t = 0$ to $t = T_e$. The strong peak in the center corresponds to the position where we have applied the

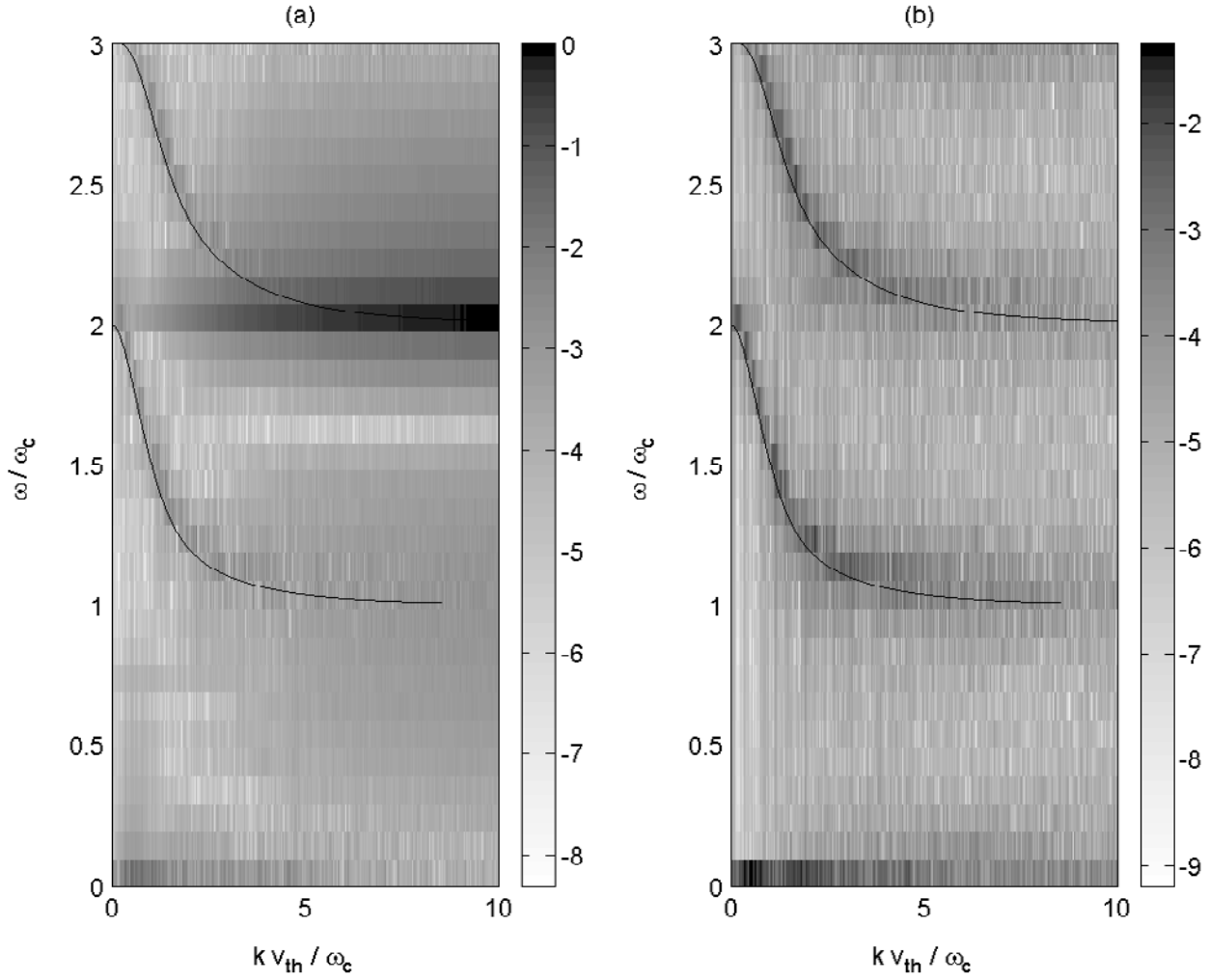

Figure 3. The power spectrum of the electrostatic (ES) waves in our particle-in-cell (PIC) simulation with the emission amplitude $E_{0,1}$ in the frequency interval $\omega < 3\omega_c$. Both plots show the wave power $\log_{10}|E(\omega, k)|^2$ normalized to the peak power in Figure 3a. Figure 3a shows the wave power in the emission time interval between $t = 0$ and $t = T_e$. The emission gives rise to the broadband structure at $\omega \approx 2\omega_c$, while we find a significant minimum of the wave power at $\omega \approx 1.5\omega_c$. In Figure 3b we show the power spectrum in the later time interval between $t = T_t - T_e$ and $t = T_t$. The transient waves of the emission have now been absorbed by the electrons, and we find waves moving on the Bernstein wave branches. In both figures the black lines show the solution of the linear dispersion relation for $\omega_p = 4\omega_c$, and which in Figure 3b accurately reproduces the Bernstein wave branches found in the simulation. See color version of this figure in the HTML.

external VNF which we consider to be the vacuum potential of the antenna. As we move away from the two cells in the center, the amplitude drops instantaneously by more than one order of magnitude. As we move further away from the antenna, we have a slower exponential amplitude drop. This is the high-frequency near field built up by the emission. For increasing values of E_0 the sheath increasingly expands into the plasma. If the sheath couples to eigenmodes of the plasma, then eventually plasma waves will develop which constitute the far field. In all plots we find that the electric field of the VNF dominates over both the near and the far fields. On the other hand, the near field covers a wider spatial interval.

[20] In Figure 5 we show the amplitude modulus as a function of space for the four electric field cases $E_{0,j}$ for the second interval between $t = T_t - T_e$ and $t = T_t$. For all four emissions we find that the VNF and the high-frequency antenna near field have damped out, which is in agreement with Figure 3. The antenna far field persists in the form of waves which have an increasing amplitude with increasing amplitudes of E_0. This antenna far field may constitute the accompanying waves that are believed to yield the strong plasma responses to sounding at ω_c and at its harmonics.

[21] To quantify the strength of the plasma response to the sounding, we compare the emission amplitudes E_0 to the maximum $E_{\max}$ of the ES field modulus for all positions and times after the emission has ended at $t = T_e$. In Figure 6 we show the logarithm of this ratio, here referred to as the antenna gain. We find that the plasma response decreases in relative strength as the emission amplitude is increased.

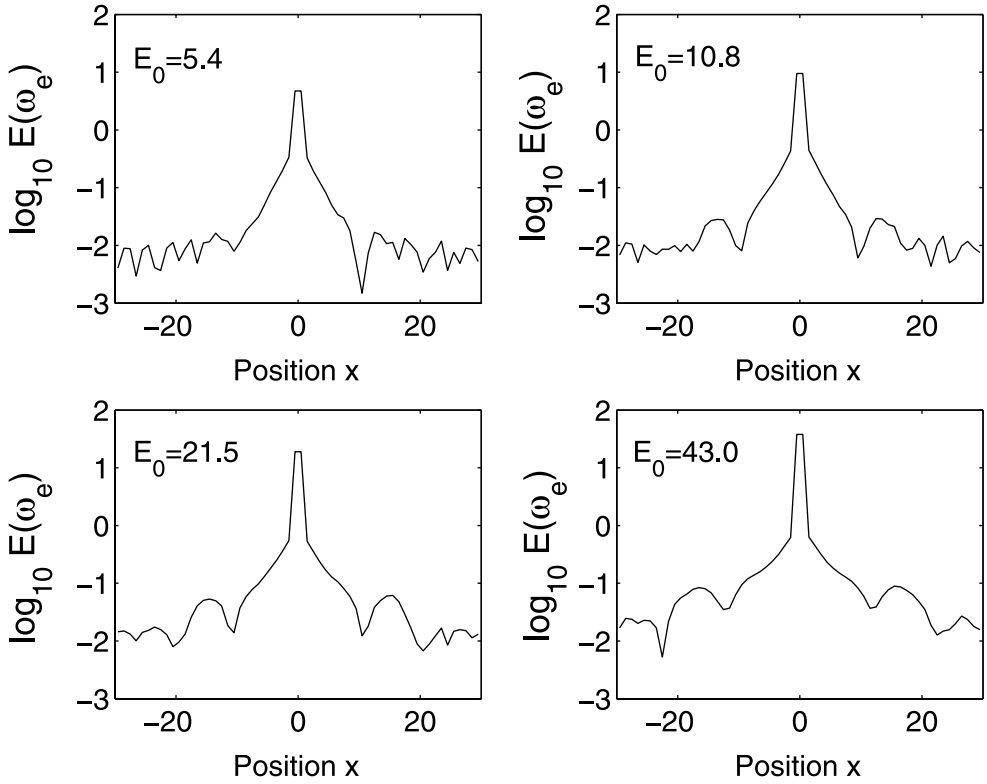

Figure 4. The electric field amplitude modulus in our box in the time interval between $t = 0$ and $t = T_e$ for the frequency ω_e and for the given values of E_0. In all four plots we find antenna sheaths forming between $x = -10$ and $x = 10$, with spatially exponentially decreasing amplitude moduli.

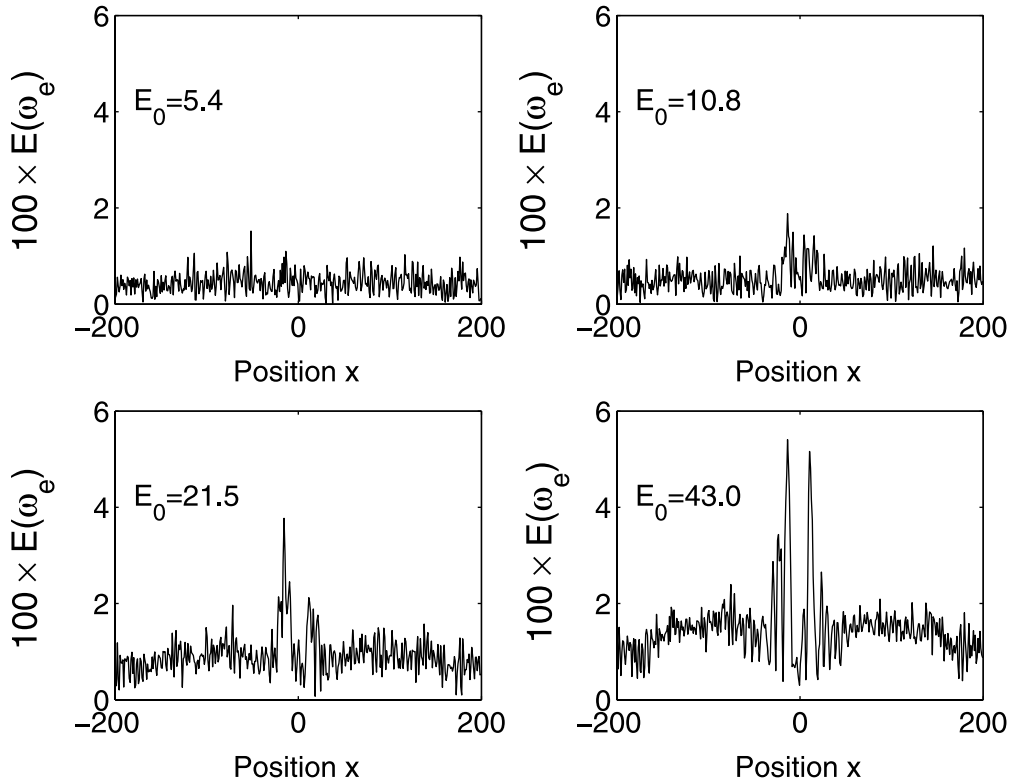

Figure 5. The electric field amplitude modulus in our box in the time interval between $t = T_t - T_e$ and $t = T_t$ for waves with the frequency ω_e and for the given values of E_0. We find that the antenna near field has damped out in all cases, while oscillating waves can be seen for all cases except for $E_{0,1} = 5.4$.

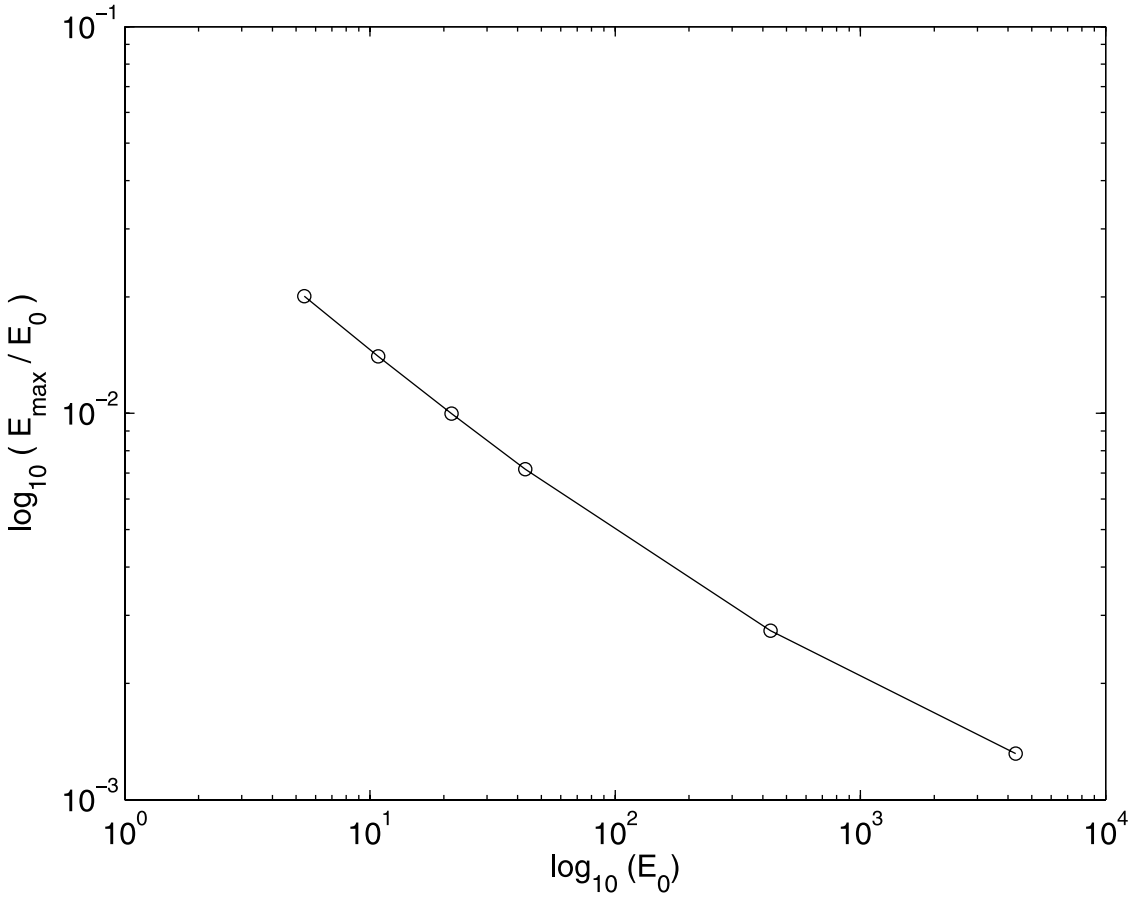

Figure 6. The maximum electric field modulus measured after the emission, normalized to the emission amplitude (antenna gain), for the emission amplitudes $E_{0,1} = 5.4$ to $E_{0,4} = 43$ and for the amplitude cases $E_0 = 430$ and $E_0 = 4300$. For the lowest amplitudes, the measured electric field response is ≈20 dB below the emission amplitude, while for the highest amplitudes, the electric field response drops to ≈30 dB below the emission amplitude.

This suggests wave absorption mechanisms like nonlinear damping [*Riyopoulos*, 1986].

[22] From Figure 2 we expect a detectable heating of the electrons by the VNF of the emission. This is confirmed by Figure 7 where we show the time evolution of the total kinetic energy of all electrons in the simulation box for four emission amplitudes, two of which we discuss in the next section. We find that the electron heating takes place until $t = T_e$. Thereafter it remains constant which implies that the oscillations in Figure 5 do not contribute to the heating. The kinetic energy increases steadily with time and its growth has not saturated until the emission end at $t = T_e$.

[23] We may estimate the peak speed that the electrons can reach by their acceleration in the VNF field as follows. We take an electron with the speed $v_\perp = 3.5$, which is the highest speed that is initialized in the PIC simulations. We fix its phase by $v_y = 0$ to fulfill condition 1 as the electron enters the antenna. From Figure 2 we find that the VNF should accelerate electrons by the speed increment $\Delta v_x = v_{x,2} - v_{x,0} \approx 0.1$ for $E_{0,1}$, by $\Delta v_x \approx 0.2$ for $E_{0,2}$, by $\Delta v_x \approx 0.4$ for $E_{0,3}$, and to $\Delta v_x \approx 0.85$ for $E_{0,4}$.

[24] Figure 8 shows the distribution of the electrons as a function of $v_\perp$ at $t = T_e$ for the four $E_{0,j}$. We have integrated the number of computational electrons over 20 simulation cells to allow for a good statistical representation. We compare this distribution to that integrated over a spatial interval that has not been affected by the emission. We find that the electrons are heated for all four $E_{0,j}$ and that the average electron speed close to the antenna increases with increasing $E_{0,j}$. The maximum speed the electrons reach is $v_\perp \approx 3.8$ for $E_{0,1}$, $v_\perp \approx 4.2$ for $E_{0,2}$, $v_\perp \approx 5.3$ for $E_{0,3}$, and $v_\perp \approx 6.5$ for $E_{0,4}$. The observed changes in $v_\perp$ during the emission are in all cases larger than those estimated from Figure 2 for a simple crossing of the antenna by the electron. Electrons can cross the antenna up to 20 times during T_e. The energy the electrons accumulate during multiple antenna crossings can explain the peak energy the electrons reach in Figure 8 at least to the correct order of magnitude. It further explains the steady growth of the electron kinetic energy in Figure 7 during the entire emission period because the final distribution in Figure 8 cannot be reached by a single pass of an electron through the antenna. Multiple antenna encounters at differing electron phase angles relative to the antenna will also impose varying electron acceleration efficiencies by the VNF, probably leading to a thermalization of the electrons, explaining the apparently Maxwellian distribution of the heated electrons in Figure 8. It is, however, not clear from

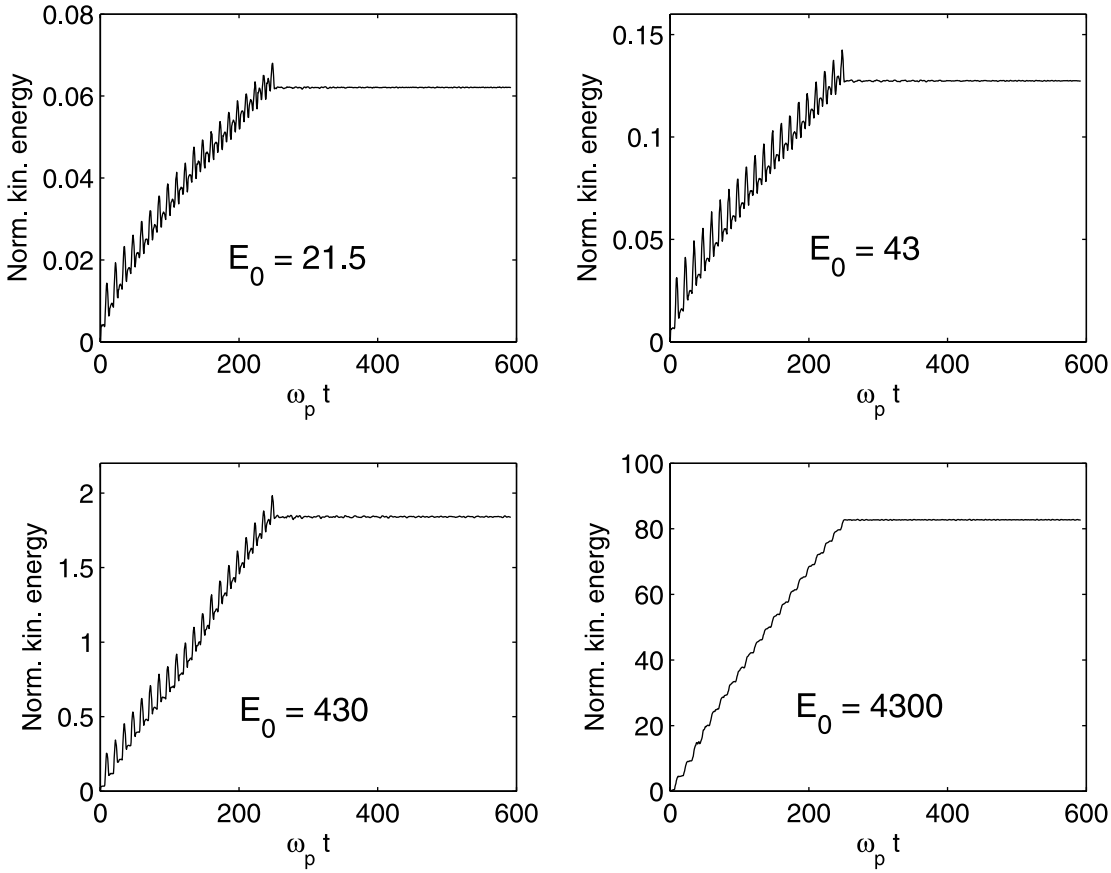

Figure 7. The change in the total kinetic energy in the simulation box as a function of the emission amplitude for $E_{0,3} = 21.5$, $E_{0,4} = 43$, $E_0 = 430$, and $E_0 = 4300$. We have normalized the energy to the total initial thermal electron energy in the box and we have then subtracted unity from all values. In all figures, the electrons gain energy during the emission by interacting with the very near field (VNF) and the near field. After the end of the emission at $\omega_p t = \omega_p T_e = 80\pi$, the kinetic energy remains constant.

this simple model why so many electrons are heated close to the antenna, since only electrons that initially have been close to the antenna will cross it due to their confinement by the orthogonal magnetic field. The observed heating must thus have a second component.

[25] To identify this component, we have to find the region in which electrons are heated. For this we examine the temporal change of the electron kinetic energy perpendicular to the magnetic field. We calculate $\Delta E = v_\perp^2(t + \Delta t) - v_\perp^2(t)$. We set $\Delta t = 0.6$, i.e., 2% of one gyroperiod. This time interval has been chosen such that the energy changes of the electrons are stronger than those due to the simulation noise and at the same time short enough to allow for a localization of the electron. During this time an electron moving at v_{th} will only move 0.6 λ_D. We show the result for the emission amplitude $E_{0,4}$ and for the time $t = 30$ in Figure 9.

[26] We find that electrons are strongly accelerated close to the antenna. The changes in the electron energy arise from a change in the antenna potential and the therefrom resulting change in the electron kinetic energy. The observed energy changes significantly exceed those given by equation (7), but we have to remember that the electrons will loose some of the kinetic energy before they leave the antenna. The equation (7) yields the net acceleration of the electron by a single crossing of the antenna potential.

[27] More importantly, however, is that we find electron acceleration also at distances up to 15 λ_D from the antenna, which matches the maximum distance from the antenna where we find a significant near field in Figure 4. We also find pronounced acceleration minima at positions ± 6 λ_D. These acceleration minima must be connected to zero-crossings of the electric field. The acceleration and thus the electric field strength envelope decreases as we move away from the antenna. Figure 9 thus suggests a spatial electric field of the type $\exp(ik|x|)$ with complex k and where $|x|$ is the modulus of the distance from the antenna. Such an electric field is typical for transiently damped wave modes. The distance of 1.5 electron thermal gyroradii v_{th}/ω_c of the first electric field minimum from the antenna gives a wave length of about $3v_{th}/\omega_c$. This gives a normalized wave number $kv_{th}/\omega_c \approx 2$ which is the lowest wave number at which Figure 3a shows significant power. Since the nonlinear Landau damping of waves increases its strength for increasing kv_{th}/ω_c, as discussed by *Riyopoulos* [1986], this is just the most weakly damped wave that can be excited by the emission and it therefore may be the wave that can expand most into the ambient plasma.

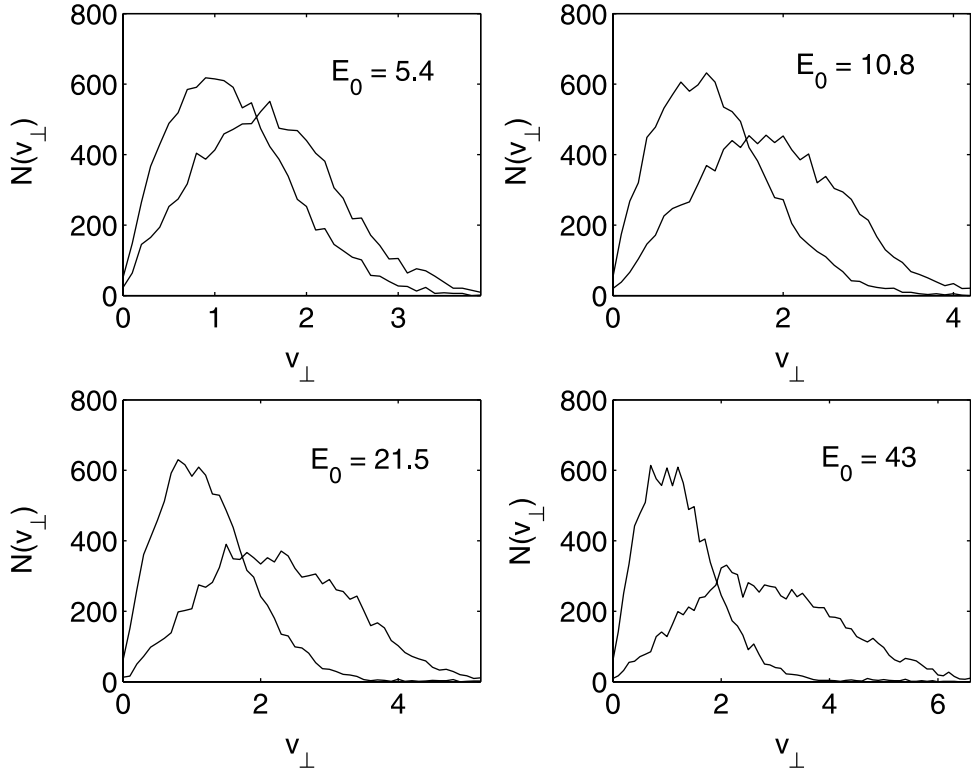

Figure 8. The velocity distribution of the electrons perpendicular to the magnetic field at time $t = T_e$ for the respective E_0. The two curves in each plot show the electron distribution integrated over the intervals between $x = -10$ to $x = 10$ in which the electrons have been heated strongest and the unperturbed spatial interval between $x = 380$ and $x = 400$. The distribution of the heated population has a density maximum at a larger speed than the unheated population. We show here only the intervals for which we found more than 10 computational electrons per speed interval.

[28] In Figure 10 we show ΔE as a function of the position at the time $t = 237$, which is close to the end of the emission at T_e. The emission amplitude is $E_{0,4}$. Here we find again substantial changes in ΔE up to a significant distance away from the antenna. The fastest electrons have a $v_\perp = 6$ and they can thus only cross the distance 3.6 λ_D during the time Δt, i.e., we find that the near fields do also at this stage substantially accelerate electrons. The steep rise of ΔE close to the antenna may be attributed to the exponential damping of the transient waves of the near field as we move away from the antenna or due to the electrons interacting with the VNF.

[29] The localized wave emission for $E_{0,4}$ has heated the electrons close to the antenna. At this stage we believe that the near fields accelerate electrons to speeds that allow electrons that are initially too far from the antenna to cross the antenna cells. This heating by the antenna near field thus expands the spatial interval in which electrons can be accelerated by the VNF, which explains the large number of accelerated electrons in Figure 8. The maximum speed that the electrons can reach is in a reasonable agreement with the estimate from equation (7) if we take into account multiple antenna crossings.

[30] An important observation is also that the size of the interval over which the electrons are accelerated in Figures 9 and 10 implies that the wave oscillations in Figure 5 are located on a temperature gradient. Since the wave length of Bernstein modes scales with the average Larmor radius of the electrons, this implies that the waves observed in Figure 5 and also in real sounding experiments may not be simple Bernstein mode waves.

4. Application to Plasma Sounders

[31] Finally, we compare our normalized plasma parameters to the parameters in physical units encountered by plasma sounders. Relaxation sounders like the WHISPER experiment on board Cluster typically apply a potential of the order of 100 V between the dipole antenna wires. Each wire is thus on a vacuum peak potential of 50 V. We assume here that this potential is similar if the antenna is immersed in a plasma. We further assume that this potential is shielded over one Debye length λ_D and that the electric field is piecewise constant within this interval which is of course only a crude approximation. A typical plasma encountered by the Cluster sounder may have a thermal speed $v_{th} \approx 5 \times 10^5$ m/s and a plasma frequency $\omega_p \approx 10^4 \times 2\pi/s$. We thus obtain a $\lambda_D \approx 8$ m for these parameters. We have a normalized $E_{0,RS} \approx 35$, which is comparable to $E_{0,4}$. We have found substantial electron heating for these parameters.

[32] The topside sounder on board OC produces antenna potentials of 550 V [*James et al.*, 1999]. A plasma the OC sounder encounters may have a thermal speed of 2×10^5 m/s and a plasma frequency of 5×10^5 $2\pi/s$. The Debye length is here $\lambda_D \approx 6 \times 10^{-2}$ m. The electric field is

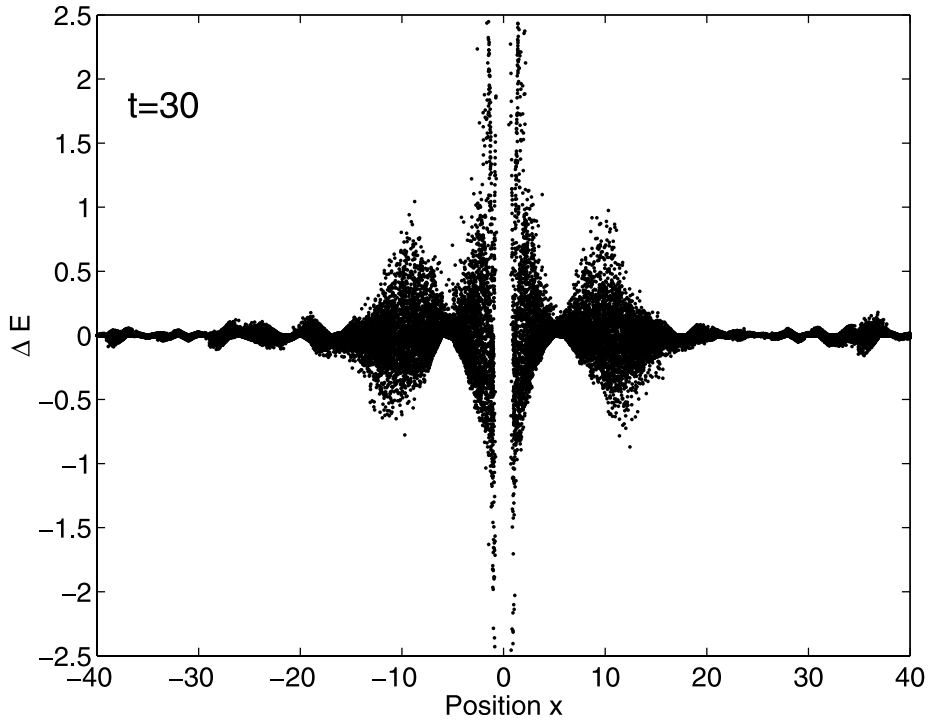

Figure 9. The change in the kinetic electron energy perpendicular to the magnetic field during a time interval of $\Delta t = 0.6$, starting at the simulation time $t = 30$, for the emission amplitude $E_{0,4} = 43.0$. We find the strongest energy changes at the antenna cells where electrons are trapped by the antenna potential. Electrons are heated at distances up to 20 λ_D from the antenna.

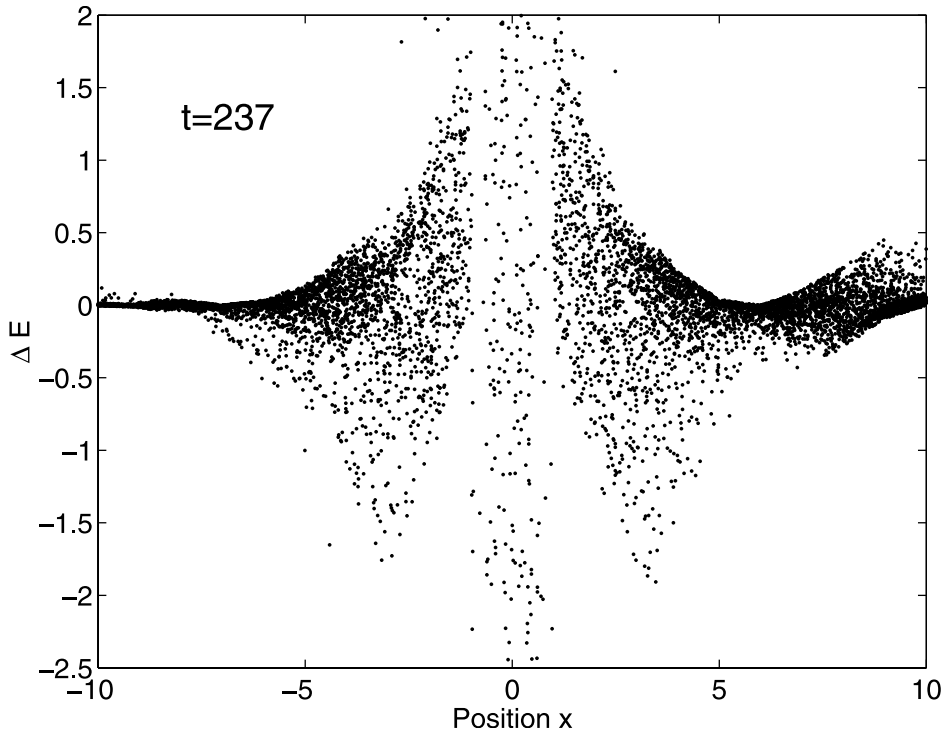

Figure 10. The change in the kinetic electron energies perpendicular to the magnetic field during a time interval of $\Delta t = 0.6$ starting at the simulation time $t = 237$ for the emission amplitude $E_{0,4} = 43.0$. Here, the strongest energy changes are found at the antenna cells where electrons are trapped by the antenna potential. Electrons are heated at distances up to 6 λ_D from the antenna to the left and even further away to the right of the antenna.

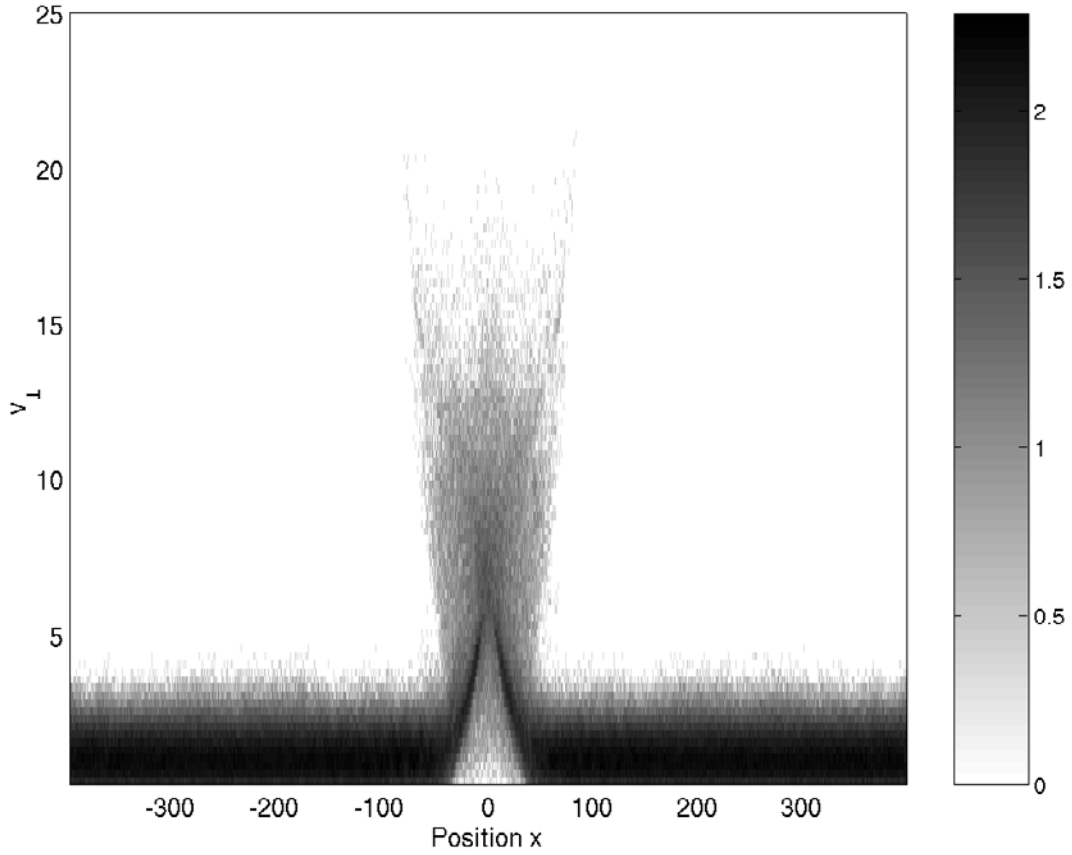

Figure 11. The electron phase space distribution after the end of an emission with the amplitude E_0 = 430 and with a duration of $T_e = 40\pi/\omega_e$. The electrons are accelerated up to $v_\perp \approx 20$ and the sheath of hot electrons extend to a distance of 100 λ from the antenna.

then $E_0 \approx 2500$. To cover the possible range of values for E_0 that may apply to the OC sounder, we perform two simulations, one with E_0 = 430 and one with E_0 = 4300. We use a total of 819,200 computational electrons over 800 simulation grid cells.

[33] In Figure 11 we show the phase space density as a function of $v_\perp$ and x after the end of an emission with E_0 = 430 which lasts 20 periods of ω_e. Electrons are accelerated up to $v_\perp \approx 20$ which is for $v_{th} = 2 \times 10^5$ m/s an electron maximum speed of 4×10^6 m/s or an energy of 45 eV. This is considerably less than the typical SAE energies between 1 keV to 20 keV. The heated electrons cover a radius of 100 λ_d or 6 m for our plasma parameters.

[34] In Figure 12 we show the electron distribution for an emission amplitude of E_0 = 4300. Here, electrons are accelerated to speeds of $v_\perp \approx 100$, resulting in peak speeds of 2×10^7 m/s or a kinetic energy of 1.1 keV. For such amplitudes, electrons are therefore accelerated to typical energies for SAE. The thickness of the sheath formed by the hot electrons is here almost 400 λ_D or 24 m. Since electrons are not likely to encounter the VNF of the antenna more than once, the maximum energy they may reach in reality is probably somewhat lower than that we find in our 1-D model, i.e., even such high emission amplitudes can not directly produce the 20 keV SAE. The important observation from the Figures 11 and 12 is however that a substantial fraction of the electrons is accelerated. These electrons yield a hot electron sheath around antennas and the beams of hot electrons we observe at large distances from the antenna in particular in Figure 12 could then drive the sheath waves discussed by *James* [1993] and *James et al.* [1995]. In the hot plasma surrounding the antenna, these sheath waves could grow to a large amplitude and produce SAE by their interaction with the already hot sheath electrons.

[35] Emissions with a frequency $\omega_e = 0.625$ and the same amplitudes as we used to accelerate the electrons in the Figures 11 and 12 produce electrons with approximately the same peak energy, i.e., the acceleration shows no strong dependence on the emission frequency as predicted by equation (7).

5. Discussion

[36] In this paper we have examined the electron acceleration by a simple antenna model both analytically and by particle-in-cell simulations, in which we have introduced an externally driven time-oscillating ES potential. We have used the simplest possible approximation to the very near field of the antenna both in deriving a map for the change of the electron speed as it crosses this field and in the PIC simulations. Our model describes a thin permeable plane with an infinite extent and with an oscillating charge density but with no oscillating currents.

[37] We have shown here that our simple antenna model leads to a map for the electron speeds that allows for their acceleration. We have then found SAEs in our PIC simu-

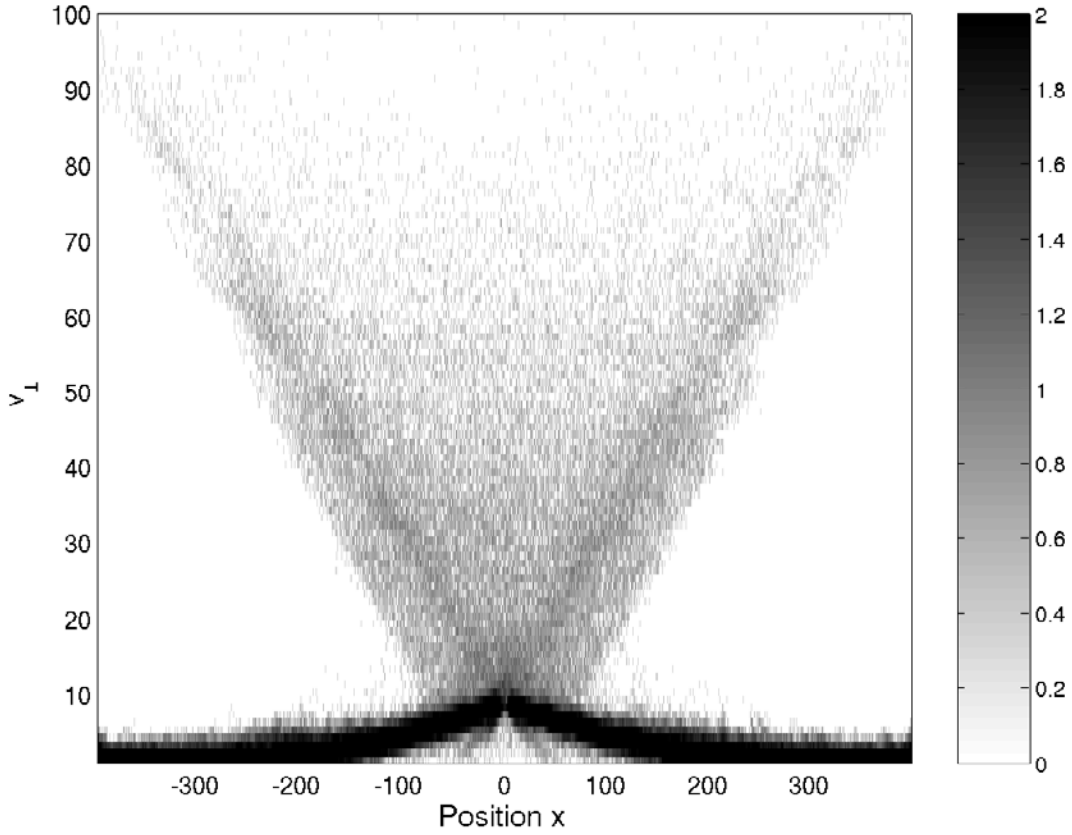

Figure 12. The electron phase space distribution after the end of an emission with the amplitude E_0 = 4300 and with a duration of $T_e = 40\pi/\omega_e$. The electrons are accelerated up to $v_\perp \approx 100$ and the sheath of hot electrons extend to a distance of 400 λ from the antenna.

lations, confirming this. As a consequence, we can now explain the previously observed electron heating where we have modeled localized plasma emissions by means of PIC simulations [*Dieckmann et al.*, 1999; *Dieckmann et al.*, 2000].

[38] We have further presented evidence for that the PIC simulation yields self-consistent antenna near and far fields, for which we cannot easily find analytic expressions or obtain experimental measurements. One particularly important aspect has been the observation in our simulations that emissions at a frequency $\omega_e = 2\omega_c$ can excite localized oscillating ES fields at this frequency, which are probably responsible for the strong plasma response to sounding at the electron gyrofrequency and at its harmonics. Important is hereby that the oscillations may not be simple Bernstein waves due to the electron temperature gradient in the plasma. A further investigation of this important issue is however beyond the scope here and is left to future work.

[39] Finally, we have compared our normalized plasma parameters to the parameters in physical units encountered by plasma sounders. We have performed simulations with emission amplitudes that are comparable to that of the relaxation sounder Whisper on board the Cluster mission, and we have found substantial electron heating for these parameters. The high mobility of the electrons along **B** should, however, rapidly carry the electrons away from the antenna making them hard to detect. This is in contrast to topside sounders since here the large electron plasma and gyrofrequencies imply short acceleration timescales, during which the electrons may not move substantially along the magnetic field direction, in particular because their thermal speed is low. The topside sounder on board OC produces antenna potentials of 550 V [*James et al.*, 1999]. Such high fields suggest a significantly stronger electron acceleration as it is the case for relaxation sounders. Our simulations have indeed shown that in this case our simple model predicts that electrons may be accelerated up to keV energies. It is, however, problematic to analytically estimate the maximum speed the electrons can acquire, since the Debye length changes substantially by the heating, which makes it difficult to set the electric field E_0 in our map.

[40] The presence of heated electrons close to the OC antenna even if the electron acceleration by the VNF field may not yield keV electrons is however an important first step for the generation of SAE. The hot electrons in the sheath surrounding the antenna allow for larger linear wave amplitudes which in turn may allow for electrons to reach the keV energies by their nonlinear interaction with the sheath waves. Any collapsing strong waves could also accelerate electrons to a higher speed. An involvement of sheath waves in the acceleration may also explain the observed increase of the acceleration efficiency if the emission frequency is equal to the frequency of a plasma eigenmode. The VNF we use here does not show any strong resonance as we see from equation (7) which implies that SAE generation must involve a further step. A verification

of this requires however multidimensional simulations which are still out of reach for the currently available computer hardware.

[41] We point out that the approximation of the VNF by piecewise constant electric fields is too simple to accurately describe the antennas on board plasma sounders, in particular because we considered one spatial dimension without making use of the cylindrical symmetry of the antenna. Giving accurate quantitative estimates for how efficiently SAEs can be generated by the OC antenna are thus beyond the work presented here. However, the analysis in this work suggests that PIC simulations may develop into practical tools for examining the properties of antennas immersed in magnetized space once the increasing computer performance routinely allows for 3-D simulations at the required resolution and for more adequate antenna models. The possibility to externally access the electric and magnetic fields at individual simulation cells opens up the possibility to introduce more realistic shapes of the potential very near to the antenna. All further antenna fields can then be calculated self-consistently. The ever-increasing computer performance will allow us in the future to perform realistic simulations in three spatial dimensions that may provide a quantitatively correct picture of antenna-plasma couplings in plasma.

[42] **Acknowledgments.** This research was partially supported by the Swedish National Supercomputer Centre (NSC), by the Deutsche Forschungsgemeinschaft (Bonn) through the Sonderforschungsbereich 591, by Linköpings University, by the European Commission (Brussels) through contract HPRN-CT-2001-00314, and by the Leverhulme trust.

[43] Shadia Rifai Habbal thanks H. Gordon James and another referee for their assistance in evaluating this paper.

References

Dieckmann, M. E., S. C. Chapman, A. Ynnerman, and G. Rowlands (1999), The energy injection into waves with a zero group velocity, *Phys. Plasmas*, *6*, 2681–2692.

Dieckmann, M. E., S. C. Chapman, A. Ynnerman, and G. Rowlands (2000), Plasma sounding at the upper hybrid frequency, *J. Geophys. Res.*, *105*, 13,103–13,117.

Dieckmann, M. E., A. Ynnerman, S. C. Chapman, G. Rowlands, and N. Andersson (2004), Simulating thermal noise, *Phys. Scripta*, *69*, 456–460.

Eastwood, J. W. (1991), The virtual particle electromagnetic particle-mesh method, *Comput. Phys. Commun.*, *64*, 252–266.

Huang, C. Y., W. J. Burke, D. A. Hardy, M. P. Gough, H. G. James, E. Villalon, and L. C. Gentile (2001), Electron acceleration by megahertz waves during OEDIPUS C, *J. Geophys. Res.*, *106*, 1835–1847.

James, H. G. (1993), Ionospheric wave emissions passively detected by the Oedipus-A tether, *J. Geophys. Res.*, *98*, 19,099–19,109.

James, H. G., K. G. Balmain, C. C. Bantin, and G. W. Hulbert (1995), Sheath waves observed on Oedipus-A, *Radio Sci.*, *30*, 57–73.

James, H. G., V. I. Sotnikov, W. J. Burke, and C. Y. Huang (1999), OEDIPUS-C observations of electrons accelerated by radio frequency fields at whistler-mode frequencies, *Phys. Plasmas*, *6*, 4058–4069.

Kellogg, P. J., and S. D. Bale (2001), Antenna-plasma and antenna-spacecraft resistance on the Wind spacecraft, *J. Geophys. Res.*, *106*, 18,721–18,727.

Pulinets, S. A., and V. V. Selegey (1986), Ionospheric plasma modification in the vicinity of a spacecraft by powerful radio pulses in topside sounding, *J. Atmos. Terr. Phys.*, *48*, 149–157.

Riyopoulos, S. (1986), Nonlinear Landau damping of purely perpendicular Bernstein modes, *J. Plasma Phys.*, *36*, 111–125.

Shuiskaya, F. K., Y. I. Galperin, A. A. Serov, N. V. Baranets, Y. V. Kushnerevsky, G. V. Vasilev, S. A. Pulinets, M. D. Fligel, and V. V. Selegey (1990), Resonant heating of the ionospheric plasma by powerful radiopulses aboard the Intercosmos-19 and Cosmos-1809 satellites, *Planet. Space Sci.*, *38*, 173–180.

Tsutsui, M., I. Nagano, H. Kojima, K. Hashimoto, H. Matsumoto, S. Yagitani, and T. Okada (1997), Measurements and analysis of antenna impedance aboard the Geotail spacecraft, *Radio Sci.*, *32*, 1101–1126.

M. E. Dieckmann, Department of Science and Technology, Linköpings University, Campus Norrköping, Sweden. (mardi@itn.liu.se)

B. Eliasson and P. K. Shukla, Institut für Theoretische Physik IV, Ruhr-Universität Bochum, D-44780 Bochum, Germany. (bengt@tp4.rub.de; ps@tp4.rub.de)

G. Rowlands, Department of Physics, University of Warwick, Coventry CV 47 AL, UK. (g.rowlands@warwick.ac.uk)